Available online at www.sciencedirect.com

ScienceDirect

Procedia IUTAM 16 (2015) 70 – 79

Procedia IUTAM

www.elsevier.com/locate/procedia

IUTAM Symposium on Dynamics of Capsules, Vesicles and Cells in Flow

Dynamics of a spherical capsule in a planar hyperbolic flow: influence of bending resistance.

C. Dupont[a,b], P. Le Tallec[b], D. Barthès-Biesel[a], M. Vidrascu[c,d], A.-V. Salsac[a,*]

[a] *Biomechanics and Bioengineering Laboratory (UMR CNRS 7338), Université de Technologie de Compiègne, CS 60319, 60203 Compiègne, France*

[b] *Solid Mechanics Laboratory (UMR CNRS 7649), Ecole Polytechnique, 91128 Palaiseau Cedex, France*

[c] *REO project-team, Inria-Rocquencourt, B.P. 105, 78153 Le Chesnay cedex, France*

[d] *REO project-team (LJLL, UMR CNRS 7958), UPMC Université Paris VI, 75005 Paris, France*

Abstract

We consider an initially spherical capsule freely suspended in a planar hyperbolic flow and study the influence of the wall bending resistance on the capsule dynamics. The capsule wall is assumed to be made of a three-dimensional homogeneous elastic material. The fluid-structure interaction between the capsule and the external flow is modeled numerically by coupling a boundary integral method with a shell finite element method. It is found that, for given three-dimensional wall mechanical properties, the capsule deformability is drastically reduced as the bending resistance is increased. But, if one expresses the same results as a function of the two-dimensional mechanical properties of the mid-surface, which is how the capsule wall is modeled in the thin-shell model, the capsule deformed shape is identical to the one predicted for a capsule devoid of bending resistance. The bending rigidity is found to have a negligible influence on the shape and deformation: the capsule main deformation mode is thus solely a function of the elastic stretching of the mid-surface. The wall bending resistance still plays a role locally in the regions where buckling occurs. Its influence is studied in the low flow strength regime, for which wrinkling of the wall is observed to persist at steady state. We show that the wrinkle wavelength only depends on the bending number, which compares the relative importance of bending and shearing phenomena, and provide the correlation law. This result is interesting as it allows bending resistance to be estimated from experiments on capsules in a planar hyperbolic flow at low flow strength.

Peer-review under the responsibility of the organizing committee of DYNACAPS 2014 (Dynamics of Capsules, Vesicles and Cells in Flow).

Keywords: spherical capsule; shell finite element method; boundary integral method; planar hyperbolic flow; wrinkling.

1. Introduction

Liquid core microcapsules are widely used in bioengineering and in pharmaceutics to protect fragile or volatile substances until their liberation in an external medium. Classically produced by interfacial polymerization of an emulsion, the fabricated capsules are quasi-spherical; their wall thickness and mechanical properties depend on the

* Corresponding author. Tel.: +33 (0)3 44 23 73 38; Fax: +33 (0)3 44 23 79 42.
E-mail address: a.salsac@utc.fr

Peer-review under the responsibility of the organizing committee of DYNACAPS 2014 (Dynamics of Capsules, Vesicles and Cells in Flow).
doi:10.1016/j.piutam.2015.03.009

reaction process used to generate the membrane[1,2,3,4]. In many applications, the capsule wall is thin to facilitate the exchanges between the internal and external media. Despite its small value, the finite thickness has an important consequence from a mechanical point of view, as it provides a bending resistance to the capsule wall.

Planar hyperbolic flows have been used to study experimentally the deformation of synthetic capsules[5,6]. It is found that an initially spherical capsule is stretched in the elongational direction and compressed in the perpendicular direction by the hydrodynamic stresses exerted by the internal and external flows. It reaches a steady state which depends on the flow strength, but is independent of the capsule internal viscosity.

To date all the numerical studies that solved the fluid-structure interactions between a capsule and a planar hyperbolic flow have treated the capsule wall as a two-dimensional surface devoid of bending resistance (membrane model)[7,8,9,10,11]. At low flow strength, they showed that wrinkling occurs in the central region during the transient phase and persists at steady state. This membrane buckling is due to compressive tensions (forces per unit curved length in the capsule surface), which occur in the plane orthogonal to the direction of elongation. As the flow strength is increased, the capsule becomes more deformed: the isotropic tensions increase and eventually overcome any compressive tension, so that buckling no longer occurs. There therefore exists a critical flow strength value, above which wrinkles no longer form at steady state. It is important to study the process of wrinkling as it may lead to local stress peaks, and thus to membrane damage. However, membrane model simulations can only predict *where* wrinkling occurs depending on the flow conditions, but do not provide information on the wrinkles themselves.

To model buckling in a rigorous way, the capsule wall bending resistance must be taken into account, but no such study has yet been conducted for capsules in hyperbolic flows. A few studies have, however, been applied to capsules in simple shear flow. Most numerical models have then modeled the capsule wall as an elastic surface and decomposed the strain energy as the sum of a membrane elastic energy and a bending energy computed from the local curvature[12,13,14]. Another approach has been to consider the membrane wall as a three-dimensional homogeneous material and to use a thin shell model. Le & Tan[15] have, for instance, developed such a thin shell model without studying the influence of bending resistance on the capsule deformation per se.

The objective of the present study is thus to model the capsule wall as a three-dimensional homogeneous material with uniform thickness and to analyze the influence of the bending resistance on the deformation of an initially spherical capsule subjected to a planar hyperbolic flow. The numerical method couples a boundary integral method (to simulate the flow of the internal and external liquids) with a shell finite element method (for the capsule wall). The problem and the numerical method are briefly described in Sections 2 and 3 respectively. The effect of the wall thickness on the capsule deformation and wrinkle formation is presented in Section 4 and discussed in Section 5.

2. Problem formulation

We consider an initially spherical capsule enclosed by a three-dimensional homogeneous incompressible wall. The capsule radius ℓ is measured at the middle of the wall thickness and is the length scale of the problem. The wall consists of a hyperelastic material with thickness $\alpha\ell$ ($\alpha < 1$), bulk shear modulus G and Poisson ratio $\nu = 1/2$. The capsule is suspended in a planar hyperbolic flow in the xy-plane with undisturbed velocity field

$$\underline{v}^{\infty} = \dot{\gamma}\,(x\,\underline{e}_x - y\,\underline{e}_y), \tag{1}$$

where $\dot{\gamma}$ is the shear rate. Since the inner fluid properties do not influence the steady-state solution, the inner and outer fluids are modeled with the same viscosity μ and density.

2.1. Wall mechanics

We assume the wall to be thin enough to be modeled as a thin shell defined by the mid-surface $\mathcal{S}_t$ at time t. It is commonly accepted in practice that the thin shell approximation is valid for $\alpha \leq 15\%$ at most. The position of a material point in the shell is defined by the independent curvilinear coordinates (ξ^1, ξ^2, ξ^3). In the reference non-deformed state (time $t = 0$), the position of a point M of the mid-surface is given by

$$\underline{OM} = \underline{\varphi}\,(\xi^1, \xi^2) \tag{2}$$

with O the curvilinear basis center. It is convenient to introduce the local covariant base $(\underline{A}_1, \underline{A}_2, \underline{A}_3)$ defined as

$$\underline{A}_\alpha = \frac{d\underline{\varphi}(\xi^1, \xi^2)}{d\xi^\alpha} = \underline{\varphi}_{,\alpha} \qquad \text{and} \qquad \underline{A}_3 = \frac{\underline{A}_1 \times \underline{A}_2}{\| \underline{A}_1 \times \underline{A}_2 \|}, \tag{3}$$

where $\underline{A}_3$ is the unit normal vector. The contravariant base $(\underline{A}^1, \underline{A}^2, \underline{A}^3)$ is defined by $A^\alpha \cdot A_\beta = \delta^\alpha_\beta$ with δ^α_β the Kronecker tensor and $\underline{A}^3 = \underline{A}_3$. The same quantities are defined in the deformed state, using lowercase letters: the local covariant and contravariant bases are respectively denoted $(\underline{a}_1, \underline{a}_2, \underline{a}_3)$ and $(\underline{a}^1, \underline{a}^2, \underline{a}^3)$. Thus, in the reference configuration, the three-dimensional position $\underline{X}$ of a material point within the capsule wall is

$$\underline{X}(\xi^1, \xi^2, \xi^3) = \underline{\varphi}(\xi^1, \xi^2) + \xi^3 \underline{A}_3 \tag{4}$$

where $|\xi^3| < \alpha\ell/2$. In the deformed configuration, the new position $\underline{x}$ of a material point differs from the original position $\underline{X}$ through an unknown displacement field $\underline{u}$:

$$\underline{x}(\underline{X}, t) = \underline{X} + \underline{u}(\underline{X}, t). \tag{5}$$

We assume that the displacement satisfies the Reissner-Mindlin kinematic assumption, i.e. a material line initially orthogonal to the mid-surface remains straight and unstretched during deformation but does not remain orthogonal to the deformed mid-surface [16]. The displacement $\underline{u}$ can then be written

$$\underline{u}(\xi^1, \xi^2, \xi^3, t) = \underline{u}_S(\xi^1, \xi^2, t) + \xi^3 \theta_\lambda(\xi^1, \xi^2, t)\, \underline{a}^\lambda(\xi^1, \xi^2). \tag{6}$$

The first term represents the displacement of a line perpendicular to the mid-surface at coordinates (ξ^1, ξ^2). The angles θ_1 and θ_2 are the rotations of this line around $\underline{a}^2$ and $\underline{a}^1$, respectively.

The deformation gradient $\underline{\underline{F}}$ is given by

$$\underline{\underline{F}} = \frac{\partial \underline{x}}{\partial \underline{X}}, \tag{7}$$

while the nonlinear Green-Lagrange strain tensor $\underline{\underline{e}}$ is defined by

$$\underline{\underline{e}} = \frac{1}{2}(\underline{\underline{F}}^T \cdot \underline{\underline{F}} - \mathbb{I}), \tag{8}$$

where $\mathbb{I}$ is the unit tensor. The Reissner-Mindlin assumption implies that $e_{33} = 0$. However, e_{13} and e_{23} are non-zero and both involve the rotation θ_λ.

The wall is considered to be made of a linear isotropic material and to follow the Hooke's law. The expression of the second Piola-Kirchhoff stress tensor $\underline{\underline{\Sigma}}$ as a function of the Green-Lagrange strain tensor $\underline{\underline{e}}$ then reads

$$\underline{\underline{\Sigma}} = 2G\left(\underline{\underline{e}} + \frac{\nu}{1-\nu}\,\mathrm{tr}\underline{\underline{e}}\right). \tag{9}$$

In the present study, we consider the geometrical non-linearities that arise under large deformation, by keeping all the non-linear terms of the strain tensor $\underline{\underline{e}}$, when it is expressed as a function of the position. This explains why we will refer to the constitutive law as the *generalized Hooke's law*. The Cauchy stress tensor $\underline{\underline{\sigma}}$ is related to the Piola-Kirchhoff stress tensor [17] by:

$$\underline{\underline{\sigma}} = \frac{1}{\det \underline{\underline{F}}}\, \underline{\underline{F}} \cdot \underline{\underline{\Sigma}} \cdot \underline{\underline{F}}^T. \tag{10}$$

It can be shown that the generalized Hooke's law is strain-hardening under uniaxial stretching.

The wall equilibrium equations to be solved are

$$\nabla \cdot \underline{\underline{\sigma}} = \underline{0} \text{ inside the wall}, \tag{11}$$

$$\underline{\underline{\sigma}} \cdot \underline{a}_3 = \underline{q}^+ \text{ on the external surface } \mathcal{S}_t^+, \tag{12}$$

$$\underline{\underline{\sigma}} \cdot \underline{a}_3 = -\underline{q}^- \text{ on the internal surface } \mathcal{S}_t^-, \tag{13}$$

where $\underline{q}^+$ (respectively $\underline{q}^-$) is the load per unit deformed area which is applied by the external (respectively internal) fluid. The wall equilibrium (Eq. 11-13) can be rewritten using the principle of virtual work as

$$\int_{\mathcal{S}_t^+} \underline{\hat{u}} \cdot \underline{q}^+ \, d\mathcal{S}_t - \int_{\mathcal{S}_t^-} \underline{\hat{u}} \cdot \underline{q}^- \, d\mathcal{S}_t = \int_V \underline{\underline{\hat{e}}} : \underline{\underline{\sigma}} \, dV, \tag{14}$$

where V is the shell wall volume in the deformed state, $\underline{\hat{u}}$ an arbitrary kinematically admissible virtual displacement and $\underline{\underline{\hat{e}}}$ the corresponding virtual strain tensor. This equation means that the work done by the external load equals the one done by the internal stresses. For thin walls, the virtual work of the external load reduces to the virtual work of the jump of viscous traction forces $\underline{q}$

$$\int_{\mathcal{S}_t^+} \underline{\hat{u}} \cdot \underline{q}^+ \, d\mathcal{S}_t - \int_{\mathcal{S}_t^-} \underline{\hat{u}} \cdot \underline{q}^- \, d\mathcal{S}_t = \int_{\mathcal{S}_t} \underline{\hat{u}} \cdot \underline{q} \, d\mathcal{S}_t. \tag{15}$$

Finally, the weak form of the wall equilibrium (14) is

$$\int_V \underline{\underline{\hat{e}}} : \underline{\underline{\sigma}} \, dV = \int_{\mathcal{S}_t} \underline{\hat{u}} \cdot \underline{q} \, d\mathcal{S}_t, \tag{16}$$

where V is the shell wall volume in the deformed state, $\underline{\hat{u}}$ an arbitrary virtual displacement in the Sobolev space and $\delta\underline{\underline{e}}$ the corresponding virtual strain tensor. Since the capsule wall is treated as a thin shell, the elastic stresses in the wall can be integrated across the thickness to yield mean tensions, which are forces per unit length acting on the mid surface, on $\mathcal{S}_t$.

The difference between the membrane and shell models for the wall is that, in the membrane model, all the terms which are $O(\alpha)$ are ignored, so that the membrane displacement is only given by $\underline{u}_S(\xi^1, \xi^2, t)$. In the shell model, the three-dimensional effects across the wall thickness are taken into account in the displacement (Eq. 6). These effects are included in the left-hand side term of Eq. (16) and lead to a resistance to bending, which is quantified by a bending modulus M_B. For a homogeneous material that follows the generalized Hooke's law (Eq. 9), M_B is given by

$$M_B = \frac{G}{6(1-\nu)} (\alpha \ell)^3. \tag{17}$$

It follows that for the same deformation of the mid-surface, the expression of the load $\underline{q}$ is different for the membrane and shell models.

2.2. Internal and external flows

Owing to the small capsule size, the Reynolds number $Re = \rho \ell^2 \dot{\gamma}/\mu$ is very small. The internal and external flows are thus governed by the Stokes equations. The velocity of the mid-surface points can be expressed as an integral equation over the deformed capsule surface $\mathcal{S}_t$ using the boundary integral method. For inner and outer fluids of equal viscosity, it reads

$$\forall \underline{x}_S \in \mathcal{S}_t, \quad \underline{v}(\underline{x}_S) = \underline{v}^\infty(\underline{x}_S) - \frac{1}{8\pi\mu} \int_{S_t} \left(\frac{\mathbb{I}}{\| \underline{r} \|} + \frac{\underline{r} \otimes \underline{r}}{\| \underline{r} \|^3} \right) \cdot \underline{q}(\underline{y}_S) \, dS, \tag{18}$$

where $\underline{v}^\infty$ is the undisturbed flow velocity. The vector $\underline{r} = \underline{x}_S - \underline{y}_S$ is the distance vector between the point $\underline{x}_S$, where the velocity vector is calculated, and a point $\underline{y}_S$ on the surface $\mathcal{S}_t$. The wall and fluid mechanics are coupled through $\underline{q}$ and through the kinematic condition, which relates the wall velocity to the time derivative of the displacement field

$$\forall \underline{x}_S \in \mathcal{S}_t, \quad \underline{v}\left(\underline{x}_S(\xi^1, \xi^2, t)\right) = \frac{\partial}{\partial t} \underline{u}_S(\xi^1, \xi^2, t). \tag{19}$$

The displacement $\underline{u}_S$ is deduced from the fluid solver by integrating Eq.(19). The other part of the displacement $\underline{u}$ corresponding to the rotational term and the load $\underline{q}$ are computed by the solid solver.

2.3. Problem parameters

The capsule dynamics are governed by the relative wall thickness α and by the bulk capillary number

$$Ca_V = \mu\dot{\gamma}/G, \tag{20}$$

which compares the viscous to the elastic forces. When the wall is very thin ($\alpha \ll 1$), it is customary to introduce a surface shear modulus $G_S = G\alpha\ell$, to which corresponds a surface capillary number

$$Ca_S = \mu\dot{\gamma}\ell/G_S = Ca_V/\alpha. \tag{21}$$

This surface capillary number is classically used to study the dynamics of capsules without bending resistance. When the bending resistance of the wall is accounted for, a bending number K_B can be introduced to measure the relative importance of bending and shearing effects:

$$K_B = \frac{M_B}{\alpha G\ell^3} = \frac{M_B}{G_S\ell^2}. \tag{22}$$

Since we consider the capsule wall to be composed of a homogeneous incompressible material, the bending number is simply $K_B = \alpha^2/3$ from Eq. (17) and the influence of the bending number can be easily observed by changing the relative wall thickness α.

3. Numerical method

To solve the fluid-structure interaction problem, we couple a shell finite element method for the capsule deformation with a boundary integral method for the internal and external flows. It is similar to the one designed by Walter *et al.*[9] to simulate the dynamics of a capsule devoid of bending resistance. However, to take into account the wall bending resistance, the wall is modeled as a thin shell with finite thickness and bending resistance.

The capsule wall is discretized with a mono-layer of linear triangular shell elements of constant thickness. The elements are generated by meshing the mid-surface of the wall of the undeformed spherical capsule. We inscribe either an icosahedron (regular polyhedron with 20 triangular faces) or an octahedron (regular polyhedron with 8 triangular faces) in the sphere. We sequentially subdivide the triangular elements and project the resulting nodes on the spherical mid-surface. The wall mesh is thus defined by the nodes located on the mid-surface.

The position of a point inside an element is represented using the local coordinates (r, s, z), where (r, s) are the intrinsic coordinates of the element mid-surface ($r, s, 1-r-s \in [0, 1]$) and z is the coordinate along the normal vector to the mid-surface ($z \in [-1, 1]$, with $z = 0$ corresponding to the mid-surface). From Eq. (4), the position vector $\underline{X}$ inside the element then reads

$$\underline{X}(r, s, z) = \sum_{i=1}^{3} \lambda_i(r, s) \left(\underline{X}_i + z\frac{\alpha}{2}\underline{A}_{3i}\right) \tag{23}$$

where λ_i are the 2D shape functions of the standard 3-node isoparametric elements at node i, $\underline{X}_i$ the position vector of the node and $\underline{A}_{3i}$ the unit normal vector at the node. The expressions of the displacement and strain tensor are then deduced from Eq. (23). An integration of the displacement across the wall thickness is performed in order to take into account the effect of the wall thickness[16].

We use shell elements of the MITC family (Mixed Interpolation Tensorial Components) with three nodes on the mid-surface (one at each vertex): they are designed to handle the modeling of objects with wall thicknesses much smaller than their characteristic size, a situation that is prone to locking phenomena. The MITC approach is based on a mixed formulation that interpolates strains and displacements separately and connects both interpolations at specific tying points.

The numerical method consists in following the Lagrangian position of the nodes of the mid-surface $\mathcal{S}_t$ at each time step. The finite element method allows us to deduce the rotational term of the displacement $\underline{u}$ (Eq. 6) by solving the virtual work principle equation (Eq. 16) by iterations using an implicit Newton method. The displacement $\underline{u}$ is obtained by summing the rotational term and the displacement $\underline{u}_S$ of the mid-surface. The solid solver allows also us

to compute the viscous load exerted by the fluids on the capsule wall from the known displacement of the membrane nodes. The membrane velocity is then obtained from the boundary integral formulation. The displacement of the mid-surface nodes $\underline{u}_S$ is calculated by integrating the velocity with an explicit Euler integration scheme.

4. Effect of wall bending resistance on capsule deformation

In the following, all the results (capsule profiles, deformation, etc.) pertain to the deformed capsule mid-surface.

We investigate the influence of the non-dimensional governing parameters on the deformation of an initially spherical capsule subjected to a planar hyperbolic flow. We first consider an initially spherical capsule with constant bulk shear modulus G at $Ca_V = 0.005$ and vary the wall thickness. Figure 1 shows that the capsule is elongated in the flow direction and compressed in the perpendicular direction at steady state. More importantly, it qualitatively indicates that the thicker the wall, the less deformed the capsule is at steady state. The capsule deformation thus decreases with the bending resistance. At steady state, the capsule assumes a quasi-ellipsoidal shape, which can be approximated by mid-surface ellipsoid of inertia. The capsule deformation can then be measured by the Taylor parameter D_{12}^{∞} defined as

$$D_{12}^{\infty} = \frac{L_1 - L_2}{L_1 + L_2}, \tag{24}$$

where L_1 and L_2 are the lengths of the two principal axes of the mid-surface ellipsoid of inertia in the xy-plane. The evolution of the Taylor parameter as a function of Ca_V and α is shown in Figure 2a. For a given wall thickness, the capsule elongates under the influence of the external flow, so that D_{12}^{∞} increases with the bulk capillary number Ca_V. The graph also proves what was observed qualitatively in Figure 1, that increasing the wall thickness decreases the global capsule deformation.

It is interesting to observe that if we now plot the Taylor parameter as a function of the surface capillary number Ca_S (Figure 2b), all the results fall onto the same curve, which corresponds to the curve found for a capsule without bending resistance. The main deformation mode of a spherical capsule is thus governed by the elastic stretching of the mid-surface. This important result validates the use of membrane model to study the capsule deformation in an external flow.

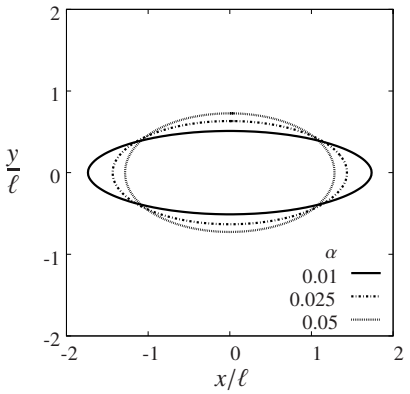

Fig. 1. Steady-state shape of the capsule mid-surface in the xy-plane for the same three-dimensional wall properties ($Ca_V = 0.05$) but different wall thicknesses α.

5. Effect of wall bending resistance on buckling

If stretching effects control the global capsule shape and deformation, bending effects may still play a role locally, whenever buckling occurs. Results obtained on capsules without bending resistance have shown that wrinkling occurs for Ca_S smaller than the critical value $Ca_{SL} = 0.14 - 0.15$. The latter is independent of the constitutive law, as the capsule deformation is then still in the small-deformation regime.

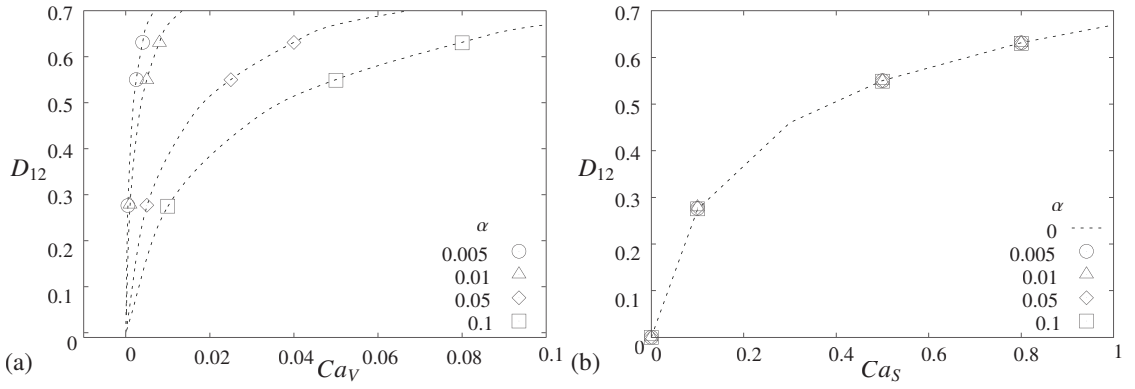

Fig. 2. Mid-surface steady deformation parameter D_{12}^{∞} as a function of Ca_V (a) and Ca_S (b) for different wall thicknesses.

In order to investigate how the bending resistance influences the formation of wrinkles, let us consider a capsule such that $Ca_S = 0.1$, which is below Ca_{SL}. The corresponding capsule thickness is varied between $\alpha = 0.003$ and 0.02, while Ca_S is kept constant, so that Ca_V is varied between 3×10^{-4} and 2×10^{-2}.

When the capsule wall is modeled as a thin shell, buckling occurs in the central region of the capsule due to compressive tensions (Figures 3b-c). Wrinkles appear at the same location as those observed when the capsule is devoid of bending resistance (Figure 3a). As was noted previously, the membrane model can thus be used to predict the location of the formation of wrinkles. But a thin shell model is needed to obtain information on the wrinkle wavelength, as it depends on the bending resistance. When the wall thickness increases, the bending resistance increases and fewer wrinkles are formed (Figures 3b-c). For $\alpha \geq 0.02$, wrinkles no longer form. It is thus possible to prevent buckling by increasing the wall thickness (Figure 3d).

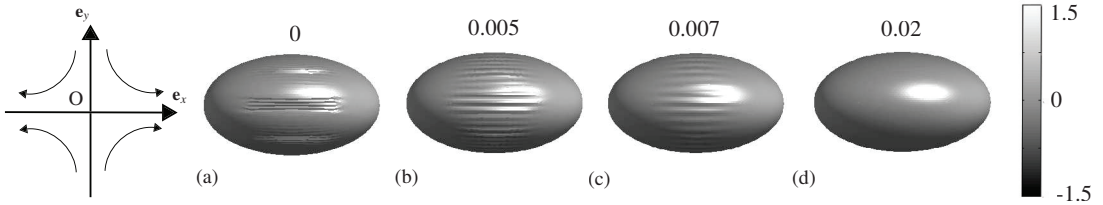

Fig. 3. Capsule shape evolution at steady state for an initially spherical capsule subjected to a planar hyperbolic flow at $Ca_S = 0.1$ with $\alpha = 0$ (a); 0.005 (b); 0.007 (c); 0.01 (d). The grey levels represent the repartition of the normal load.

Before analyzing any further the wrinkle characteristics, one first needs to ensure that the wrinkles are independent of the mesh. We consider three mesh refinements: 1280, 8192 and 20480 elements. To determine the geometric characteristics of the wrinkles (wavelength, amplitude), we compute the mid-surface cross-section within the yz-plane and subtract from it the intersection of the mid-surface ellipsoid of inertia within the same plane. The radius difference $\triangle\rho/\ell$ between the two curves is plotted as a function of the arc length s/ℓ along the mid-surface intersection (Figure 4). The wrinkle wavelength λ_e/ℓ, defined as the distance between two successive extrema, is determined for the wrinkles located near the xz-plane ($s/\ell \in [-1, +1]$). Figure 5 shows the mean wrinkle wavelength λ_e/ℓ for a capsule with $\alpha = 0.01$ and $Ca_S = 0.1$ as a function of the number of elements. The wavelength initially decreases as the mesh is refined. It reaches the constant value $\lambda_e/\ell = 0.25$ for meshes with at least 8000 elements. All the simulations have been run with 20480 elements.

The influence of the bending resistance on the wrinkle wavelength and amplitude is studied by increasing the relative wall thickness (Figure 6). Figure 6a shows that the wavelength monotonously increases with α, until wrinkles no longer form ($\alpha > 0.02$ for $Ca_S = 0.1$). The $\alpha = 0$ case corresponds to the membrane solution (no bending resistance): a wavelength of $\lambda_e/\ell \sim 0.1$ is found, which is equal to about twice the mesh size. Figure 6b indicates that the wrinkle amplitude A/ℓ is maximum for small values of α and then decreases until being nil for $\alpha > 0.02$.

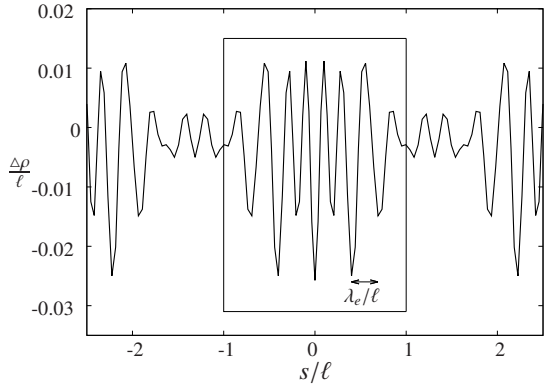

Fig. 4. Capsule meshed with 8192 elements and a relative thickness $\alpha = 0.01$ at $Ca_S = 0.1$: Radius difference $\triangle\rho/\ell$ between the intersection of the capsule mid-surface within the yz-plane and that of the ellipsoid of inertia as a function of the contour arc length s/ℓ ($s = 0$ for $y = 0$).

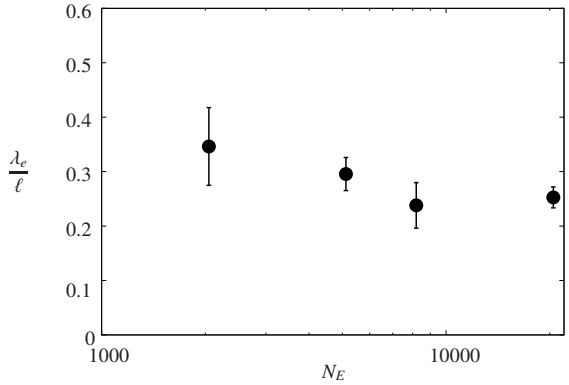

Fig. 5. Influence of the number of elements N_E on the mean wrinkle wavelength for $Ca_S = 0.1$ and $\alpha = 0.01$.

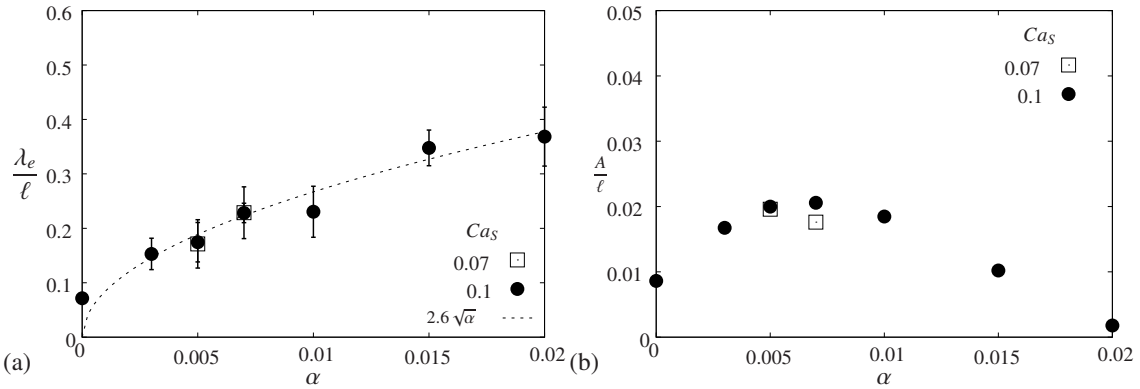

Fig. 6. Influence of the shell thickness on the mean wrinkle wavelength (a) and amplitude (b). The dashed line is the $2.6\sqrt{\alpha}$ correlation curve.

To investigate whether the surface capillary number affects the wrinkle wavelength, we have considered the case of a capsule with a thickness $\alpha = 0.005$ and 0.007 at $Ca_S = 0.07$. The two points, added in Figure 6, are superimposed on the ones found for $Ca_S = 0.1$. The wrinkle wavelength is thus not a function of Ca_S and only depends on the bending number. Still, the critical relative wall thickness above which wrinkles no longer form decreases with the surface capillary number. This is due to the fact that the capsule wall tension increases with the capillary number.

6. Discussion and conclusion

For the first time, the influence of the bending resistance on the dynamics of an initially spherical capsule with a three-dimensional homogeneous wall subjected to a planar hyperbolic flow has been studied using a numerical method coupling a boundary integral method and a shell finite element method. We show that if we consider capsules with the same three-dimensional wall mechanical properties but different thicknesses, the capsule is less deformed when the bending resistance increases. However, if we consider now capsules with the same mid-surface mechanical properties, the bending resistance marginally influences the capsule deformation. The capsule deformation and shape are thus principally governed by the in-plane mid-surface tensions. The fact that an initially spherical capsule can only deform (at constant volume) by increasing its surface area can explain why no significant effect of the bending resistance is observed under constant Ca_S. If we are not interested in the post-buckling behavior, membrane models allow us to properly model the deformation and the shape of an initially spherical capsule for a reasonable computational time.

The bending rigidity is likely to have a more significant effect in the case of an ellipsoidal capsule subjected to a simple shear flow. Ellipsoidal capsules have indeed been shown to exhibit two distinct dynamics with a transition from a solid-like tumbling motion to a fluid-like swinging mode that is governed by the energy of deformation [18]. One can expect the bending resistance to influence the energy barrier. No similar phenomenon, however, exists in the case of a planar hyperbolic flow.

It is an interesting result that the membrane model can be used to determine the capsule deformation despite the formation of wrinkles in the central region of the capsule at low flow strength. The membrane model can even predict the location where the wrinkles appear. But a thin shell model is needed to get the wrinkle characteristics. As shown in Fig. 6, the wrinkle wavelength depends only on the bending number regardless the value of the surface capillary number: it is thus a function of the square-root of the thickness ratio α. A correlation $\lambda_e/\ell = 2.6\sqrt{\alpha} = 3.4\,K_B^{1/4}$ is found with correlation coefficient $R^2 = 0.97$. It is interesting to note that, when a thin homogeneous membrane is stretched between two clamps, the wavelength of the wrinkles forming in the central region follows the law $\lambda_e/\ell = 2.9\sqrt{\alpha} = 3.8\,K_B^{1/4}$, as shown Cerda and Mahadevan [19]. In the two cases, the wrinkle wavelength depends on the bending resistance following a power law with power equal to 1/4. The small difference between the factors of proportionality is due to the difference in geometry and boundary conditions. This shows that the wavelength of the wrinkles forming along the capsule can be predicted from a simple energy balance between bending and stretching under the constraint of the constitutive law of the wall material. However, if this balance is relatively simple to establish analytically for a flat membrane, it is much harder to find for a spherical membrane subjected to viscous shear forces. A numerical model is thus necessary in this latter case.

This correlation law provides a technique to determine the surface shear modulus, the bending modulus and the wall thickness of an artificial capsule from experimental images through inverse analysis. If one subjects an initially spherical capsule at low flow strength and captures images of the capsule deformed profile, the capsule deformation parameter D_{12} can be measured on the images and used to deduce the surface capillary number Ca_S using Figure 2b (i.e. evolution of D_{12} as a function of Ca_S). Knowing the experimental value of the shear rate $\dot{\gamma}$ and the viscosity of the external fluid μ, the surface shear modulus G_S can be easily deduced from the definition of Ca_S (Eq. 21). If the wrinkles appear clearly enough on the image, there is the possibility to measure their wavelength in the central region. The relative wall thickness ratio can then be estimated from the constitutive law $\lambda_e/\ell = 2.6\sqrt{\alpha}$ and the bending modulus deduced from it. The present study thus provides a direct application for the mechanical characterization of the mechanical properties of microcapsules.

Acknowledgements

This research was funded by Ecole Polytechnique (PhD scholarship of Claire Dupont), the Conseil Régional de Picardie (MODCAP grant), the French Ministère de la Recherche (Pilcam2 grant) and the French Agence Nationale de la Recherche (CAPSHYDR grant ANR-11-BS09-013, Labex MS2T ANR-11-IDEX-0004-02).

References

1. Edwards-Lévy, F., Andry, M.C., Lévy, M.C.. Determination of free amino group content of serum albumin microcapsules: II. effect of variations in reaction time and in terephthaloyl chloride concentration. *Int J Pharm* 1994;**103**(3):253 – 257. URL: http://www.sciencedirect.com/science/article/pii/0378517394901759. doi:10.1016/0378-5173(94)90175-9.
2. Xiang, Z.Y., Lu, Y.C., Zou, Y., Gong, X.C., Luo, G.S.. Preparation of microcapsules containing ionic liquids with a new solvent extraction system. *React Funct Polym* 2008;**68 (8)**:1260 – 1265.
3. Chu, T.X., Salsac, A.V., Leclerc, E., Barthès-Biesel, D., Wurtz, H., Edwards-Lévy, F.. Comparison between measurements of elasticity and free amino group content of ovalbumin microcapsule membranes: Discrimination of the cross–linking degree. *J Colloid Interf Sci* 2011;**355**(1):81 – 88. URL: http://www.sciencedirect.com/science/article/pii/S0021979710013160. doi:10.1016/j.jcis.2010.11.038.
4. Koleva, I., Rehage, H.. Deformation and orientation dynamics of polysiloxane microcapsules in linear shear flow. *Soft Matter* 2012;**8**:3681 – 3693.
5. Chang, K.S., Olbricht, W.L.. Experimental studies of the deformation and breakup of a synthetic capsule in extensional flow. *J Fluid Mech* 1993;**250**:587 – 608.
6. de Loubens, C., Deschamps, J., Georgelin, M., Charrier, A., Edward-Lévy, F., Leonetti, M.. Mechanical characterization of cross–linked serum albumin microcapsules. *Soft Matter* 2014;**10**:4561 – 4568.
7. Dodson, W.R., Dimitrakopoulos, P.. Spindles, cusps, and bifurcation for capsules in Stokes flow. *Phys Rev Lett* 2008;**101**(20):208102 (pages 4). doi:10.1103/PhysRevLett.101.208102.
8. Lac, E., Barthès-Biesel, D., Pelakasis, A., Tsamopoulos, J.. Spherical capsules in three-dimensional unbounded stokes flows: effect of the membrane constitutive law and onset of buckling. *J Fluid Mech* 2004;**516**:303–334.
9. Walter, J., Salsac, A.V., Barthès-Biesel, D., Le Tallec, P.. Coupling of finite element and boundary integral methods for a capsule in a Stokes flow. *Int J Num Meth Engng* 2010;**83**:829 – 850.
10. Dimitrakopoulos, P.. Effects of membrane hardness and scaling analysis for capsules in planar extensional flows. *J Fluid Mech* 2014;**745**:487 – 508.
11. Dodson, W.R., Dimitrakopoulos, P.. Properties of the spindle–to–cusp transition in extensional capsule dynamics. *EPL* 2014;**106**:48003.
12. Hang, W.X., Chang, C.B., Sung, H.J.. Three–dimensional simulation of elastic capsules in shear flow by the penalty immersed boundary method. *J Comput Phys* 2012;**231**:3340 – 3364.
13. Le, D.V.. Effect of bending stiffness on the deformation of liquid capsule enclosed by thin shells in shear flow. *Phys Rev E* 2010;**82**:016318.
14. Kessler, S., Finken, R., Seifert, U.. Swinging and tumbling of elastic capsules in shear flow. *J Fluid Mech* 2008;**605**:207 – 226.
15. Le, D.V., Tan, Z.. Large deformation of liquid capsules enclosed by thin shells immersed in the fluid. *J Comput Phys* 2010;**229**:4097 – 4116.
16. Chapelle, D., Bathe, K.J.. *The Finite Element Analysis of Shells – Fundamentals.* Computation Fluid and Solid Mechanics; 2003.
17. Barthès-Biesel, D., Diaz, A., Dhenin, E.. Effect of constitutive laws for two dimensional membranes on flow-induced capsule deformation 2002;**460**:211 – 222.
18. Walter, J., Salsac, A.V., Barthès-Biesel, D.. Ellipsoidal capsules in simple shear flow: prolate versus oblate initial shapes. *J Fluid Mech* 2011;**676**:318 – 347.
19. Cerda, E., Mahadevan, L.. Geometry and physics of wrinkling. *Phys Rev Lett* 2003;**90**(7):074302. doi:10.1103/PhysRevLett.90.074302.